PCCP

Accepted Manuscript

ROYAL SOCIETY OF CHEMISTRY

www.rsc.org/pccp

Clarifying the Role of Ru in Methanol Oxidation at $Ru_{core}@Pt_{shell}$ Nanoparticles

Ehab N. El Sawy[a,b], Hany A. El-Sayed[a,b], and Viola I. Birss[a,*]
[a] Department of Chemistry, University of Calgary, 2500 University Drive N.W. Calgary, Alberta, Canada T2N 1N4
[b] Permanent Address: Physical Chemistry and Corrosion Laboratory, National Research Center (NRC), Dokki, Cairo, Egypt
* To whom correspondence should be addressed; E-mail: birss@ucalgary.ca

Abstract

The catalytic activity of $Ru_{core}@Pt_{shell}$ nanoparticles (NPs) towards CO oxidation, a strongly adsorbed intermediate that compromises the performance of direct methanol fuel cells, is known to be significantly better than at Pt alone. However, a systematic study aimed at understanding the beneficial effect of Ru on Pt during the methanol oxidation reaction (MOR) has not been carried out as yet. Here, $Ru_{core}@Pt_{shell}$ NPs, having a controlled Pt_{shell} coverage of zero to two monolayers and two different Ru_{core} sizes (2 and 3 nm), were synthesized using the simple polyol method to determine the precise role and impact of Ru on the MOR in 0.5 M H_2SO_4 + 1 M methanol at RT – 60 ^oC. Because the structure of our $Ru_{core}@Pt_{shell}$ NPs is known with such certainty, we were able to shown here that the rate of methanol adsorption/dehydrogenation can be accelerated either by compression of the Pt_{shell} (by making the Ru_{core} larger) when it is less than one monolayer in thickness, or by decreasing the electronic effect of the Ru_{core} on the Pt_{shell} (achieved by adding a second Pt layer to the Pt_{shell}). At low overpotentials, decreasing the Pt_{shell} thickness also serves to increase the rate of the MOR by enhancing the rate of oxidation of adsorbed CO. Finally, it is shown that the bi-functional effect of Ru on the Pt_{shell} plays only a minor role in the catalysis of the MOR, especially at large particles where CO surface diffusion is facilitated.

Keywords: $Ru_{core}@Pt_{shell}$ NPs, strain effect, bi-functional effect, electronic effect, methanol oxidation, formic acid oxidation, catalyst design.

1. Introduction

Many Pt-M (M = transition metal) alloys have been investigated for their catalytic activity towards the methanol oxidation reaction (MOR)[1], including Pt-Ni[2-4], Pt-Ru[5-9], and Pt-Ir[10-15]. The addition of a second metal is believed to affect the Pt activity in several ways, including enhancing the ability to adsorb OH at a lower potential than at Pt (bi-functional effect)[7, 16], manipulating the electronic properties of Pt to weaken CO adsorption (electronic or ligand effect)[17-20], and/or by changing the Pt-Pt atomic distance (strain effect)[21-23].

Pt-Ru is considered to be one of the most active catalysts for the MOR[24, 25]. The catalytic role of Ru has been explained as arising from the bi-functional mechanism and/or an electronic effect, but the literature is not conclusive on this point[26-29]. Therefore, the construction of $Ru_{core}@Pt_{shell}$ nanostructures, where both the Ru core size and Pt shell thickness can be controllably varied, should help to clarify this issue. Further, Ru is known to be susceptible to dissolution under direct methanol fuel cell (DMFC) operating conditions [30-34] and hence the fabrication of catalysts in which Ru would be protected by an overlying Pt shell is another benefit of this work.

Core@shell NPs have been shown to possess high catalytic activities towards CO oxidation [35-38], oxygen reduction [39, 40], NO_x reduction [41], etc., but only a few reports have focussed on supported and unsupported core@shell NPs, targeted specifically for methanol oxidation [11, 21, 29, 42-46]. $Ru_{core}@Pt_{shell}$ NPs, in particular, have attracted great interest due to their high catalytic activity towards CO oxidation, compared to traditional Pt-Ru alloy NPs[37], with studies having addressed the change in the catalytic activity of Ru@Pt NPs towards CO oxidation with heat treatment[47], Ru core size[38, 48], and Pt shell thickness, both in the

presence[49] and absence of H_2[48]. According to a DFT study[37] and most prior experimental work [37, 38, 48, 49], the enhancement in the CO oxidation rate occurs as a result of the modification of the electronic properties of the Pt surface atoms by the subsurface Ru_{core} atoms. However, after heat-treatment of the Ru@Pt NPs, resulting in Ru alloying at the surface, a further enhancement in the rate of CO oxidation at the Ru@Pt NPs was observed[47], related to either the electronic or bi-functional effect of Ru on the Pt surface atoms.

The bi-functional, electronic, and strain effects of the Ru core on the activity of Ru@Pt NPs towards CO oxidation was examined in our recent work, which involved controllably varying the Ru core size and the thickness of the Pt shell [48]. When the Pt shell was less than one monolayer (ML) in thickness, a single CO stripping peak was seen (0.62 V vs. RHE)[48]. This indicated that the Pt activity towards CO oxidation is controlled entirely by strong electronic interactions between the two metals. When 1-2 monolayers of the Pt shell were present, two CO stripping peaks appeared due to the presence of two types of Pt atoms, each having different electronic properties [48]. However, once a complete 2 ML Pt shell was realized, a single CO stripping peak was obtained at a more positive potential than that of the single peak obtained for the $\leq$ 1 ML Pt, as the electronic effect of Ru on the second layer of Pt atoms is buffered by the underlying Pt [23]. On the other hand, the CO oxidation process was shown to be independent of the Ru core size [48].

In terms of the activity of Ru@Pt NPs towards the MOR[29,45], Muthuswamy et al reported that the Pt:Ru ratio in Ru@Pt shell NPs increased with increasing solution pH during the encapsulation of the Ru core with Pt, according to X-ray Photoelectron Spectroscopy (XPS) results[29]. The NPs with what was assumed to be the highest degree of Pt-Ru alloying in the shell layer showed the highest MOR activity, suggesting that both the

bi-functional and electronic effects of Ru are relevant, but with the bi-functional effect being dominant. However, XPS analysis is not always accurate when analyzing NPs, as the depth from which the photoelectrons are emitted extends to several nm[50, 51], and hence determining the degree of PtRu alloying in the shell is difficult.

Here, we focus on distinguishing the impact of the electronic and strain effects imposed on the Pt shell by the underlying Ru core, as well as the bi-functional effect of Ru on Pt, during the MOR, trying to understand the extent of each effect separately. To achieve these goals, $Ru_{core}@Pt_{shell}$ NPs with a Ru_{core} exactly 2 or 3 nm in diameter and an accurately known Pt_{shell} coverage from 0 to 2 MLs[48] were studied in 0.5 M H_2SO_4 + 1 M methanol at RT – 60 ^oC. The Pt_{shell} strain (compressive, in this case) was found to greatly enhance the methanol adsorption/dehydrogenation step, but did not significantly affect the CO oxidation step. On the other hand, the electronic effect of Ru on Pt was found to inhibit the methanol adsorption/dehydrogenation step and enhance the CO oxidation rate, while the bi-functional effect was found to have only a minor impact, overall, in enhancing the MOR kinetics.

2. Experimental methods

2.1. $Ru_{core}@Pt_{shell}$ nanoparticle synthesis

The Ru_{core} NPs were synthesized using $RuCl_3.3H_2O$ (Aldrich, 99.98%) and ethylene glycol (EG, Alfa Aesar, 99%) or 1,5-pentanediol (pentamethylene glycol (PMG), Alfa Aesar, 97%) as both the solvent and reducing agent, with polyvinyl pyrrolidone (PVP, Alfa Aesar, M.W. of 40K) used as the capping agent. EG and PMG were selected due to their different boiling points (190 °C and 230 °C, respectively), shown to produce different Ru core sizes,

giving an average diameter of ~ 2 nm and ~ 3 nm when EG and PMG were used as the solvent, respectively [48].

The $Ru_{core}@Pt_{shell}$ NPs, with Pt shell coverages ranging from 0 to 2 monolayers (MLs), were synthesized by the addition of an exact number of moles of Pt precursor (*x* g $H_2PtCl_6.6H_2O$ (Sigma Aldrich, 99.9%) + 10 ml EG/PMG) to a controlled volume and concentration of the Ru NP colloidal solution. The relationship between the Pt salt concentration employed and the expected number of Pt MLs deposited around the Ru core NPs was thoroughly explained in our previous study [48]. In the case of the 2 nm dia Ru_{core} (EG) NPs, Ru:Pt molar ratios of 1:1 and 1:2.4 were found to be necessary to form one and two monolayers of Pt_{shell} on a Ru_{core} NP, respectively[48], while in the case of Ru_{core} (PMG) NPs with a diameter of 3 nm, Ru:Pt molar ratios of 1:0.6 or 1:1.4 are necessary to deposit one or two monolayers of the Pt_{shell}, respectively[48]. The details of the procedures used to synthesize the Ru_{core} and $Ru_{core}@Pt_{shell}$ NPs were given in our previous study[48].

The $Ru_{core}@Pt_{shell}$ NPs were collected in the form of a fine powder in order to determine their composition (in atomic % of each of Ru and Pt) and crystal structure. A [$Ru_x@Pt_y$ (n ML_{Pt}, EG/PMG)] notation was used, where x and y in represent the bulk Ru and Pt (at %) content, respectively, n is the number of Pt monolayers, and EG and PMG refer to the solvent used for the synthesis[48].

2.2. Characterization of Ru_{core} and $Ru_{core}@Pt_{shell}$ NPs

Transmission electron microscopy (TEM, Hitachi H-7650, Microscopy and Imaging Facility (MIF), University of Calgary) was used to determine the size of the $Ru_{core}@Pt_{shell}$ NPs. The TEM samples were prepared by diluting the NP colloidal solutions with ethanol,

and then placing one drop of the diluted solution on one side of a carbon-coated Cu TEM grid.

Powder X-ray Diffraction (PXRD, Rigaku Multiflex X-ray Diffractometer, Department of Geosciences, University of Calgary) with CuK_{α} radiation (λ = 1.5406 nm, V = 40 kV, and I = 20 mA) was used to determine the NP crystal structure. Thermogravimetric Analysis (TGA, Mettler-Toledo StarE, Department of Chemistry, University of Calgary) was performed in air from room temperature to 1000 ^{o}C, using a ramp rate of 10 ^{o}C/min, in order to accurately determine the $Ru_{core}@Pt_{shell}$ NP loading on VC.

2.3. Electrochemical studies

For the electrochemical studies, a $Ru_{core}@Pt_{shell}$ NPs/Vulcan Carbon (VC) powder, with a NP:VC mass ratio of 1:9, was prepared[48]. Standard three-electrode circuitry, using an EG&G PARC 173 potentiostat combined with a PARC 175 function generator, was employed for all of the electrochemical measurements. Data were collected using a PowerLab/400 data acquisition system and plotted with Chart for Windows v5. In this work, a two-compartment glass cell was used, where the working (WE) and counter (CE) electrodes were placed in the main compartment and the reference electrode was in the second compartment, connected to the main compartment through a Luggin capillary. For the high temperature measurements, the temperature was controlled by water circulation through the jacket of the WE compartment, using a HAAKE FS thermos-bath system[52].

The WE consisted of a 7 mm diameter glassy carbon (GC) rod, embedded in a Teflon holder and covered with a thin film of the NP/VC mixture. Ca. 20 µl of the $Ru_{core}@Pt_{shell}$ NP/VC ink[52] was deposited onto the WE (GC) surface via a 2-20 µl micropipette and

allowed to dry at room temperature. The CE consisted of a platinized Pt gauze, while the reference electrode (RE) was a reversible hydrogen electrode (RHE), to which all potentials are referred in this work. All solutions were prepared using Analar-Grade chemicals and triply distilled water. The solutions were thoroughly deaerated by bubbling N_2 gas through the solution for 15 min prior to each experiment.

3. Results and Discussion

3.1. Physicochemical Properties of $Ru_{core}@Pt_{shell}$ NPs

The synthesis of the $Ru_{core}@Pt_{shell}$ nanoparticles (NPs), having a controlled Pt shell coverage (0-2 monolayers), was achieved here by simply varying the Ru:Pt atomic ratio in the synthesis solution, similar to what was reported previously [48]. Notably, the formation of individual Ru and Pt NPs or a Pt-Ru alloy, rather than $Ru_{core}@Pt_{shell}$ NPs, was excluded in our previous study[48], based on both electrochemical and XRD measurements.

Figure 1 shows the TEM images of $Ru_{64}@Pt_{36}$ (1.0, PMG (pentamethylene glycol)) NPs, as an example, at both low and high magnifications. The NPs are seen to be spherical in shape with an average size of 3.5 ± 0.8 nm. The difference between these $Ru_{64}@Pt_{36}$ NP diameters and the size of the Ru_{core} (3 nm) [48] is only 0.5 nm, which is very close to the theoretical thickness of one monolayer of the Pt_{shell} (0.55 nm for 2 Pt atoms, one on each side of the NP). These findings confirm the formation of the expected Ru@Pt core@shell structures and validate the method used in our previous study to calculate their size [48].

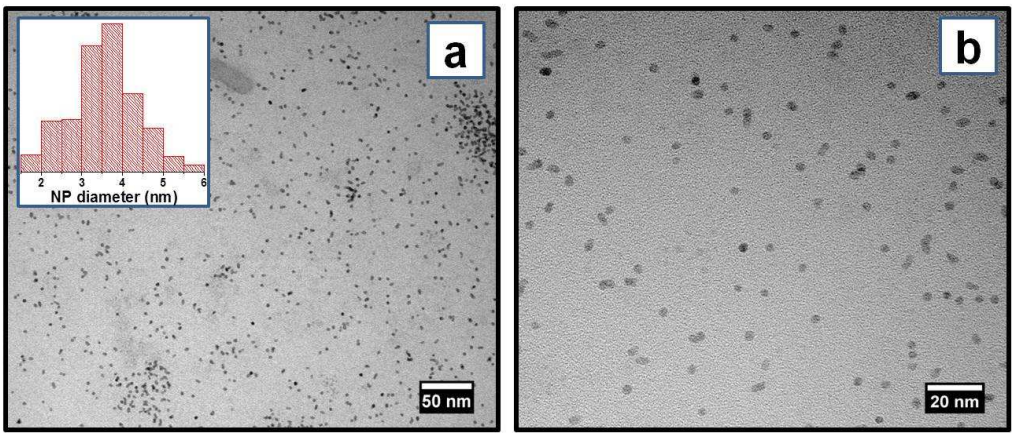

Figure 1: TEM bight field images of $Ru_{64}@Pt_{36}$ (1.0, PMG (pentamethylene glycol)) NPs, deposited on a carbon-coated Cu grid at (a) lower and (b) higher magnifications. The NP diameter histogram is given in the inset in (a).

In order to monitor the changes in the Ru@Pt NP crystal structure as the Pt shell coverage was gradually increased, Powder X-ray Diffraction (PXRD) analysis was employed[48]. The main Ru XRD peak (101) should appear at 44.01°, while the main Pt peak (111) should be at 39.89°, indicating that the Pt-Pt interatomic distance is expected to be larger than the Ru-Ru distance. The difference between these interatomic distances could result in Pt_{shell} compression, due to the strong Ru core strain effect on the shell, or to Ru_{core} expansion, due to the strong strain effect of the Pt shell on the Ru core, with the outcome depending on the size of the Ru core and the amount of Pt in the shell[23, 45, 53].

Schlapka et al[23] studied the effect of lattice mismatch between a bulk Ru(0001) substrate and heteroepitaxial Pt layers (2.5%), reporting that the surface strain remained constant and gradually decreased after five or more Pt layers had been deposited. Chen et al[45] reported TEM images that showed the presence of significantly distorted lattice fringes that resulted from accommodating a Pt shell on a highly disordered Ru core. The spacing of the

fringes was found to increase from 2.24 Å to 2.26 Å with increasing Pt shell coverage from 1.5 to 3.6 MLs, respectively, noting that the Pt lattice spacing is normally 2.265 Å[45].

Figure 2a shows the XRD patterns of the Ru_{core} and some of the $Ru_{core}@Pt_{shell}$ NPs that were prepared using EG or PMG as the solvent and reducing agent, all with a similar Pt_{shell} coverage (given in brackets). In the case of the pure Ru NPs (EG or PMG), the XRD patterns show an overlap between the peaks for the (100) plane (at 38.39°), the (002) plane (at 42.15°), and the (101) plane (at 44.01°). This is due to the broadening of the main peak (101), indicating that the Ru core in both cases (EG and PMG) contains still smaller crystallites, as reported previously by us [48] and other groups [53].

In the case of the $Ru_{core}@Pt_{shell}$ (EG) NPs, as the Pt shell coverage increases from 0.43 to 1.5 MLs, the Pt (111) and (200) XRD peaks are seen to develop, while the Ru (101) peak decreases in size until it totally disappears (Fig. 2a). These gradual changes in the XRD patterns of the $Ru_{core}@Pt_{shell}$ (EG) NPs, transitioning from that of Ru to more like Pt, may indicate the gradual expansion of the Ru_{core} lattice (accompanied by a gradual relaxation of Pt in the shell) as the Pt_{shell} coverage increases [23]. However, in the case of the $Ru_{core}@Pt_{shell}$ (PMG) NPs, the XRD patterns are similar to those of the Ru (PMG) NPs (Figure 2a), even with an increasing Pt shell coverage from 0.5 to 1.5 MLs. This indicates that, even with an increasing Pt shell coverage, essentially no change occurs in the interatomic distances within the small Ru_{core}, whereas a measureable degree of Pt_{shell} lattice compression, which does not change further with Pt shell coverage, does take place.

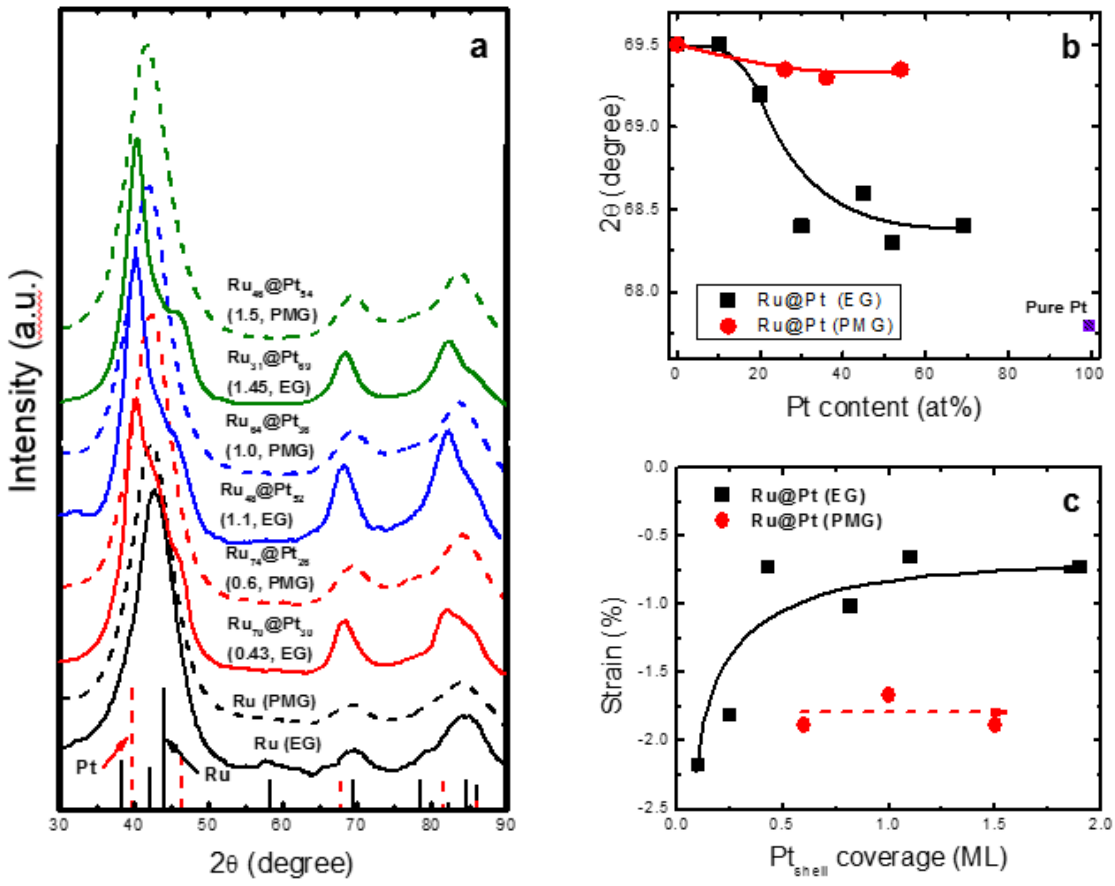

Figure 2: (a) Powder XRD patterns of $Ru_{core}@Pt_{shell}$ NPs in the 2θ range of 30°-90°. The solid and dashed vertical lines represent the 2θ value of the Ru HCP (PDF#06-0663) and Pt FCC (PDF#87-640) crystal phases, respectively. (b) Pt (220)/Ru (110) peak position of the Ru@Pt NPs (EG) and (PMG) for different Pt contents (shell coverages). (c) Comparison between the change in the Pt-Pt interatomic strain for the $Ru_{core}@Pt_{shell}$ (EG) and $Ru_{core}@Pt_{shell}$ (PMG) nanoparticles, determined by XRD analysis, as a function of Pt_{shell} coverage in monolayers.

In order to evaluate the interatomic Pt-Pt strain and follow the relaxation of the Pt shell (going from highly compressed to less compressed), the d-spacing of the $Ru_{core}@Pt_{shell}$ NP composition (Pt_{shell} coverage) was calculated using the Pt (220) XRD peak position (Figure 2b) and Bragg's Law[54], with the strain then calculated using equation [1] [22, 55].

$$\mathrm{Strain}_{Pt-Pt} = \frac{d_{Pt-Pt}\mathrm{NPs} - d_{Pt-Pt}\mathrm{Bulk}}{d_{Pt-Pt}\mathrm{Bulk}} \times 100 \qquad [1]$$

Figure 2c shows the Pt-Pt strain (negative sign indicates compression) of the $Ru_{core}@Pt_{shell}$ NPs (both EG and PMG) as a function of Pt coverage. In the case of the $Ru_{core}@Pt_{shell}$ (EG) NPs, having a 2 nm diameter Ru core, the extent of Pt shell compression decreases with increasing Pt_{shell} coverage up to ≈ 0.5 ML and then no significant further change in the strain value was observed. However, in the case of the $Ru_{core}@Pt_{shell}$ (PMG) NPs (3 nm Ru core size), a more negative strain value (more compression) in the Pt shell is seen (Figure 2c). In addition, this high degree of interatomic Pt-Pt compression for the PMG-derived NPs was found to be unaffected by the Pt_{shell} coverage.

It is important to note that the Ru_{core} formed using PMG has about three times more atoms (number of moles) than those in the smaller Ru_{core} NPs formed using EG [48]. The larger size of the PMG-derived Ru_{core} allows it to resist the change in lattice spacing due to the addition of the Pt_{shell}, as compared to the smaller Ru_{core} (EG) NPs. Therefore, in the case of the $Ru_{core}@Pt_{shell}$ (PMG) NPs, the degree of Pt-Pt compression did not change with increasing Pt shell coverage, while in the case of the $Ru_{core}@Pt_{shell}$ (EG) NPs, a gradual expansion of the Ru_{core}, accompanied by a gradual relaxation of the Pt_{shell}, is observed.

3.2. Methanol oxidation activity of $Ru_{core}@Pt_{shell}$ NPs

There are a number of possible origins of the observed catalytic activity of Ru on Pt in $Ru_{core}@Pt_{shell}$ NPs towards the methanol oxidation reaction (MOR). One of these is the bi-functional effect, arising from the situation when both the Ru and Pt sites are in contact with the solution (i.e., when the Pt_{shell} coverage is less than one monolayer (ML)) [26]. Another factor could be related to the CO surface mobility, which is crucial for CO oxidation and is

known to decrease with decreasing Pt particle size[56]. Thus, restricted CO mobility could be present at core-shell NPs with low Pt shell coverages. Another possible factor is the strain (compression) that develops within the Pt_{shell} layer as it deposits on the Ru_{core} [21, 39] due to the mismatch between the Pt and Ru lattice dimensions, as discussed above (Fig. 2). Finally, there may also be an electronic (or ligand) effect of the underlying Ru_{core} on the Pt_{shell} surface atoms [28]. The impact of each of these effects can be varied by controllably changing the Pt_{shell} coverage (0 to 1 monolayer), the Ru_{core} size, and the Pt_{shell} thickness (1 to 2 monolayers), as was done in this work and is discussed below.

3.2.1. Methanol oxidation at $Ru_{core}@Pt_{shell}$ NPs with a Pt_{shell} coverage of 0 to 1 ML

As the methanol adsorption/dehydrogenation step in the MOR requires an ensemble of three adjacent Pt atoms [57, 58], any decrease in the Pt-Pt interatomic distance in the shell layer should facilitate the breakage of the C-H bond during methanol oxidation, resulting in an overall increase in the rate of the MOR. The compressive strain in the Pt_{shell} is also known to cause a down-shift in its d-band center, resulting in weaker Pt-adsorbate interactions [21-23]. However, our previously reported CO stripping results[48] and other theoretical studies[23] have shown that Pt_{shell} compression results in only minor changes in the electronic properties of the shell compared to the more significant electronic effect of the core (Ru, in our case) on the Pt_{shell} properties.

According to the bi-functional mechanism, the optimum surface composition should provide sufficient Pt sites to maximize the methanol adsorption/dehydrogenation rate, as well as the required number of Ru atoms to remove any adsorbed CO by reaction with adsorbed

oxygen-containing species, e.g., RuOH [57]. It is important to note that the OH adsorption sites do not have to be adjacent to the site at which CO is formed, as CO is known to have a high rate of diffusion along the Pt surface [59]. However, the CO diffusion rate does depend on the size of the two-dimensional Pt islands within the shell [56] (studies have shown that Pt monolayers deposit through the formation of Pt islands that coalesce at high coverage[60]).

In order to first determine if there is a significant bi-functional effect of the Ru_{core} on the catalytic activity of the Pt_{shell} for the MOR, the methanol oxidation activity of the $Ru_{core}@Pt_{shell}$ NP catalysts was examined by covering the Ru_{core} for the first time with a controllably varied Pt_{shell} coverage of 0 to 1 ML, thus exposing both the Ru and Pt atoms to the methanol-containing solution. Figures 3a and 3b show the cyclic voltammograms of the Ru_{core} and $Ru_{core}@Pt_{shell}$ (EG) NPs (0.05-0.9 V vs. RHE, 20 mV/sec) in 1 M CH_3OH + 0.5 M H_2SO_4 at RT and 60 °C, respectively. It is well known that Ru alone has almost no catalytic activity towards the MOR[52] and hence the MOR current was normalized to only the Pt mass, also knowing that only Pt is present in the shell layer[48].

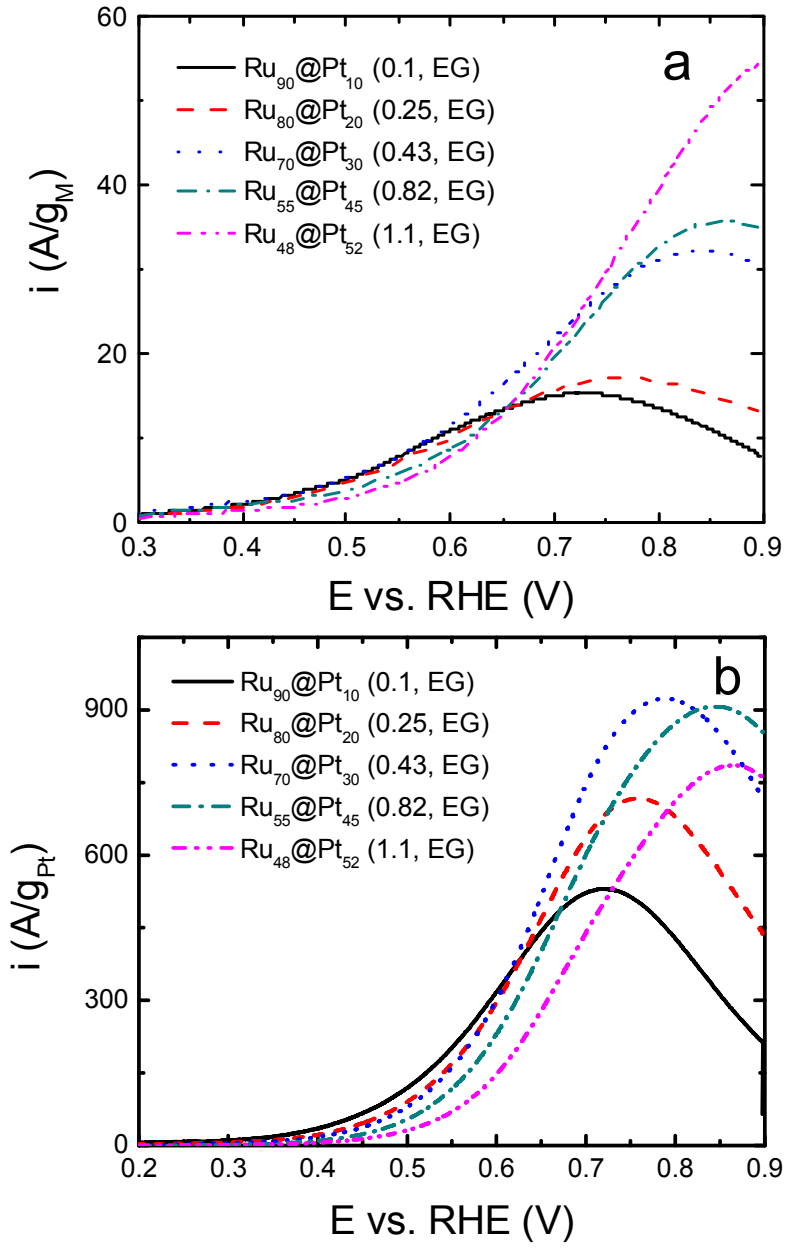

Figure 3: Methanol oxidation currents observed at Ru NPs/VC and $Ru_{core}@Pt_{shell}$ (EG) NP/VC catalysts at (a) RT and (b) 60 °C. The MOR currents were collected in the second CV (20 mV/sec) between 0.3 and 0.9 V vs. RHE in 1 M CH_3OH + 0.5 H_2SO_4 and were then divided by the Pt mass.

Figures 3a shows that, at RT the catalytic activity of the $Ru_{core}@Pt_{shell}$ (EG) NPs decreases at low potentials (0.6 V vs. RHE) and increases at higher potentials (0.8 V vs.

RHE), with increasing Pt coverage up to one ML Pt ($Ru_{48}@Pt_{52}$). At 60 ^{o}C, Figure 3b shows similar trend to what was seen at RT except at high potentials, as the catalytic activity was seen to increase with increasing Pt coverage up to 0.43 ML Pt ($Ru_{70}@Pt_{30}$) then decreases with further Pt coverage. Notably, at high temperatures, the MOR activity at the $Ru_{core}@Pt_{shell}$ NPs is expected to be significantly higher than at RT due to the increased rate of both methanol adsorption and CO desorption [61]. Consistent with this prediction, Figure 3 shows that the MOR activity has increased by an overall factor of 15-30 times at 60 °C vs. at RT, as expected.

The increase in the Pt coverage, from sub-monolayer to a full monolayer, results in a gradually increasing Pt-Pt interatomic distance (less compression) in the Pt_{shell} (Figure 3), a decrease in the exposed Ru_{core} surface area, and an increase in the Pt island size within the Pt_{shell}. Therefore, the catalytic activity of the $Ru_{core}@Pt_{shell}$ (EG) NPs could be influenced by any one of these factors, i.e., the changing Pt-Pt distance in the Pt_{shell}, the bi-functional effect of the Ru_{core} on the Pt shell, or the size of the Pt domains in the shell layer, while the electronic effect of the Ru_{core} on the Pt shell should remain constant.

At low potentials (Figures 3a (RT) and 3b (60 °C)), the methanol oxidation activity is seen to decrease with increasing Pt coverage (0-1 ML), explained by the relaxation of the interatomic Pt-Pt compression within the Pt_{shell} (Figure 3). This is because the rate of the methanol adsorption/dehydrogenation reaction decreases with increasing Pt-Pt interatomic distance. However, at higher potentials (> 0.6 V vs. RHE), the catalytic activity of the $Ru_{core}@Pt_{shell}$ NPs increases with increasing Pt coverage up to one monolayer, but only at room temperature, conditions under which the CO production rate is expected to be low. At high Pt shell coverages (the size of the Pt islands within the shell layer should then be

relatively large), the rate of CO surface diffusion/oxidation would also be expected to increase. The combined effect of these two factors is believed to be the cause of the observed enhancement in the rate of the MOR at high potentials.

Notably, even though the degree of exposure of the Ru_{core} changes with coverage of the first Pt shell layer, no evidence for the bi-functional effect of Ru was obtained at RT. However, at 60 °C (Figure 3b), an optimum activity is seen for a Pt shell coverage of 0.43 ML ($Ru_{70}@Pt_{30}$). The fact that this is very close to a Pt:Ru surface atomic ratio of 1:1 may suggest the possibility of a bi-functional effect of Ru on the catalysis of the MOR at these higher temperatures. Under these conditions, the rate of methanol oxidation, and hence the CO production rate, is significantly higher than at RT. Also, rapid Ru-OH production/regeneration is known to take place [62]. Therefore, the rate of CO diffusion/oxidation may not be sufficient to continuously regenerate clean Pt sites, while the bi-functional effect of Ru could enhance CO removal and the regeneration of the Pt sites, which, in turn, will increase the rate of methanol adsorption.

At low Pt shell coverages (< 0.25 ML), adsorbed CO may build-up rapidly due to the small area of Pt on which CO can diffuse. At medium Pt coverages, a larger Pt area is now available for CO diffusion, which results in rapid Pt site regeneration and hence enhanced methanol oxidation. Also, the presence of sufficient Ru sites for OH adsorption and the fast regeneration of adsorbed OH[62] will accelerate CO removal and the regeneration of the Pt sites, thus increasing the overall rate of methanol adsorption [63]. At close to 1 ML Pt shell coverage on the Ru core, the number of Ru-based OH adsorption sites is now quite small and the OH regeneration rate would thus be too slow to match the high rate of CO production, resulting in slow CO removal. Also, the small particle size could inhibit the rate of CO

diffusion/oxidation, especially at these temperatures, where the CO production rate is relatively high.

In order to help determine whether CO surface diffusion/oxidation and/or the bi-functional effect of exposed Ru sites are playing a major role in the activity of the Ru@Pt NPs towards methanol oxidation, the Pt coverage was varied without changing the Pt-Pt distance within the Pt_{shell} layer. This was achieved by utilizing the larger (3 nm) $Ru_{core}@Pt_{shell}$ (PMG) NPs at which a change in the Pt coverage is not associated with a change in the interatomic distances within the Pt_{shell} (Figure 3). Therefore, the MOR activity of the $Ru_{core}@Pt_{shell}$ (PMG) NPs was compared at a Pt_{shell} coverage of 0.6 versus 1 monolayer.

Figure 4 shows the cyclic voltammograms (0.05-0.9 V vs. RHE, 20 mV/sec) of the $Ru_{74}@Pt_{26}$ (0.6, PMG) and $Ru_{64}@Pt_{26}$ (1.0, PMG) NPs in RT 1 M CH_3OH + 0.5 M H_2SO_4, with the inset showing the analogous data at 60 °C. At low potentials (< 0.6 V vs. RHE), an insignificant change in the catalytic activity was observed at both low and high temperatures, with Pt coverage increase. However, at higher potentials (> 0.6 V vs. RHE), the $Ru_{74}@Pt_{26}$ (0.6, PMG) catalyst showed significantly lower activity than the $Ru_{64}@Pt_{36}$ (1.0, PMG) NPs at both low and high temperatures.

At low potentials, due to the similarity between the Pt-Pt atomic distance in both the $Pt_{74}@Pt_{26}$ (0.6, PMG) and $Ru_{64}@Pt_{36}$ (1.0, PMG) NPs, the methanol adsorption/dehydrogenation rate is also the same. Thus, the MOR activity is indistinguishable for these two catalysts and no evidence is seen for either the bi-functional effect of the exposed Ru atoms or of CO diffusion/oxidation rate limitations. At higher potentials and/or high temperatures, the rate of methanol oxidation is relatively high and thus the rate of CO production is also high. The low activity exhibited by the $Pt_{74}@Pt_{26}$ (0.6,

PMG) NPs indicating a minor (or absence of) Ru bi-functional effect and could be explained by the relatively small Pt surface area available for facile CO surface diffusion compared to $Ru_{64}@Pt_{36}$ (1.0, PMG) NPs. Therefore, the coverage of adsorbed CO at the $Pt_{74}@Pt_{26}$ (0.6, PMG) NPs is higher than at the $Ru_{64}@Pt_{36}$ (1.0, PMG) NPs, resulting in a lower MOR activity. These results indicate that CO diffusion on the Pt shell surface plays a more important role in the MOR than does the bi-functional effect of Ru, especially at the larger $Ru_{core}@Pt_{shell}$ NPs due to facilitated diffusion of CO.

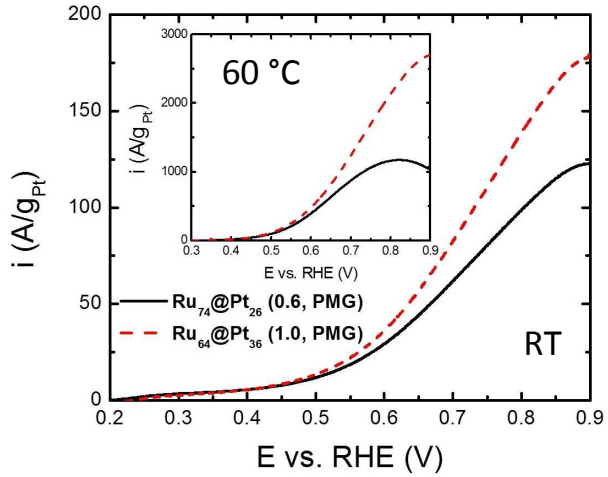

Figure 4: MOR activity of $Ru_{core}@Pt_{shell}$ NP/VC (PMG) catalysts in the second CV (20 mV/sec) between 0.3 and 0.9 V vs. RHE in 1 M CH_3OH + 0.5 H_2SO_4 at RT and 60 °C (inset).

3.2.2. Methanol oxidation at $Ru_{core}@Pt_{shell}$ NPs with a Pt_{shell} coverage of one ML

In the case of both the $Ru_{core}@Pt_{shell}$ (1.1, EG) and $Ru_{core}@Pt_{shell}$ (1.0, PMG) NPs, the Ru_{core} is covered with close to one full monolayer of Pt, as confirmed by our previous study on these materials [48], and therefore the bi-functional effect cannot play a role in the MOR at these catalysts. However, the Pt–Pt interatomic compression in the $Ru_{core}@Pt_{shell}$ (1.0, PMG) NPs is higher than in the case of $Ru_{core}@Pt_{shell}$ (1.1, EG) (Figure 3) due to the different sizes of the Ru_{core} (3 and 2 nm, respectively. Based on these facts, any differences in the catalytic

activity of these $Ru_{core}@Pt_{shell}$ (1.1, EG) and $Ru_{core}@Pt_{shell}$ (1.0, PMG) NPs, with a full ML coverage of Pt, must be related to the difference in the Pt-Pt interatomic distances in the Pt_{shell}, as this is the only difference between these two core-shell materials.

Figure 5 shows the cyclic voltammograms (0.05-0.9 V vs. RHE, 20 mV/sec) of the $Ru_{core}@Pt_{shell}$ (1.1, EG) NPs and $Ru_{core}@Pt_{shell}$ (1.0, PMG) NPs in 1 M CH_3OH + 0.5 M H_2SO_4 at both room temperature and 60 °C (Inset of Figure 5). The $Ru_{core}@Pt_{shell}$ (1.0, PMG) NPs that have a highly compressed Pt_{shell} are seen to have a higher catalytic activity towards the MOR than the $Ru_{core}@Pt_{shell}$ (1.1, EG) NPs at RT by a factor of 4.4 at low potentials (0.6 V vs. RHE) and 3.5 at higher potentials (0.8 V vs. RHE). At 60 °C, these differences are 3.3 and 3 at lower and higher potentials, respectively.

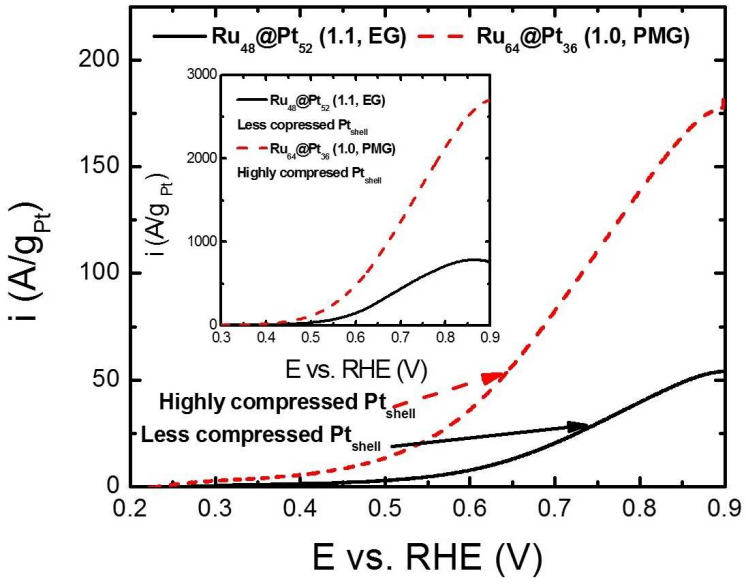

Figure 5: The effect of the Pt-Pt interatomic distance in the Pt_{shell} (determined by the size of the Ru core) on the MOR activity of Ru@Pt/VC catalysts with a close to one monolayer Pt shell coverage. The catalytic activity was obtained in the second CV (20 mV/sec) between 0.05-0.9 V vs. RHE in 1 M CH_3OH + 0.5 M H_2SO_4 at RT and 60 °C (inset).

The change in the Pt-Pt atomic distance as the Ru core size was altered but the Pt shell was fixed at one monolayer coverage could cause both strain and electronic effects[21-23]. Therefore, in order to determine the main cause of the enhancement in the MOR rate for the larger Ru core size NPs (Figure 5), another reaction that requires more than one Pt atom for the adsorption and oxidation steps (i.e., formic acid oxidation[64, 65]) was examined (Scheme 1). The results obtained (Figure 6) were compared with the CO stripping reaction (Figure 6, inset), which involves the linear adsorption of CO on Pt (i.e., one CO molecule per Pt atom) and is very sensitive to the electronic properties of Pt.

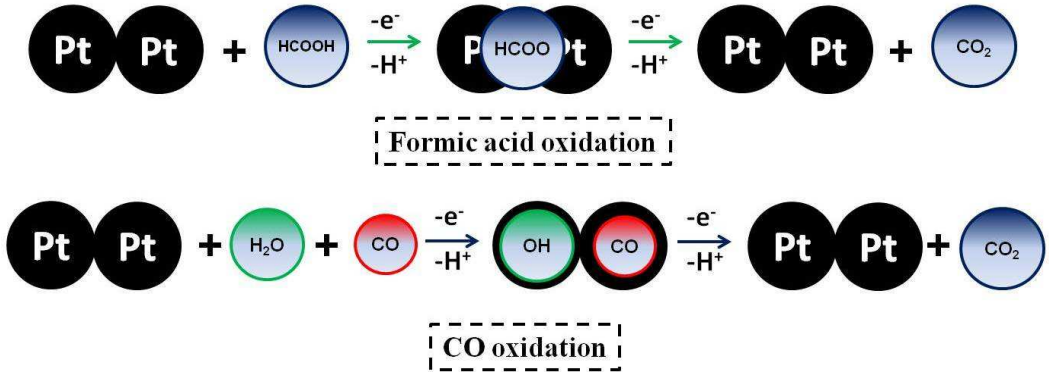

Scheme 1: The required number and orientation of Pt surface atoms required for (top) formic acid oxidation and (bottom) CO oxidation (stripping).

Figure 6 shows the cyclic voltammograms (0.05 - 0.9 V vs. RHE, 20 mV/sec) of the $Ru_{48}@Pt_{52}$ (1.1, EG) and $Ru_{64}@Pt_{36}$ (1.0, PMG) NP catalysts in 1 M HCOOH + 0.5 M H_2SO_4 at 60 °C. As expected from the methanol oxidation results (Figure 5), the $Ru_{64}@Pt_{36}$ (1.0, PMG) NPs with the larger Ru core size show a higher catalytic activity towards formic acid oxidation than do the smaller Ru core $Ru_{48}@Pt_{52}$ (1.1, EG) NPs by a factor of ca. 2.4 at both low and higher potentials. However, the CO stripping behaviour (onset and peak

potentials) seen at the $Ru_{48}@Pt_{52}$ (1.1, EG) and $Ru_{64}@Pt_{36}$ (1.0, PMG) NPs was found to be almost the same, as shown in the inset of Figure 6.

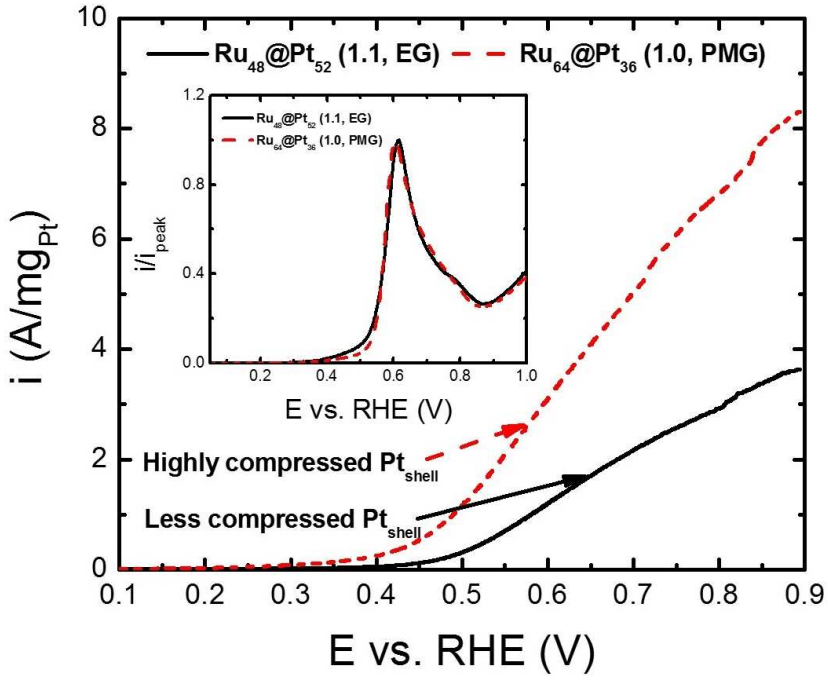

Figure 6: The effect of the Pt-Pt interatomic distance in the Pt_{shell}, dictated by the size of the Ru core (2 nm in case of EG and 3 nm in the case of PMG)) on the $Ru_{core}@Pt_{shell}$ NP/VC catalytic activity towards formic acid oxidation. The currents were collected in the second CV (20 mV/sec) between 0.05 - 0.9 V vs. RHE in 1 M HCOOH + 0.5 H_2SO_4 at 60 °C. Inset: Effect of Pt-Pt interatomic distance in the Pt_{shell} on the $Ru_{core}@Pt_{shell}$ NP/VC catalyst activity towards CO stripping in 0.5 H_2SO_4 at RT (20 mV/sec).

The CO stripping results (Fig. 7 inset) confirm that, for both the $Ru_{48}@Pt_{52}$ (1.1, EG) and $Ru_{64}@Pt_{36}$ (1.0, PMG) NPs, which have different Pt-Pt interatomic distance dictated by the smaller and larger Ru core sizes, respectively (Figure 3), the electronic properties of the Pt atoms in the Pt_{shell} are almost the same. Therefore, there is no effect of the compression of the Pt shell on the CO oxidation kinetics in either case. On the other hand, the oxidation of methanol (Fig. 6) and formic acid (Fig. 7), which require three and two adjacent Pt atoms, respectively, are both significantly affected by the Pt-Pt distance in the Pt_{shell}. These results

confirm that the higher MOR activity of the $Ru_{core}@Pt_{shell}$ (1.0, PMG) NPs, compared to that of the $Ru_{core}@Pt_{shell}$ (1.1, EG) NPs (Figure 5), is related to the enhancement of the methanol adsorption/dehydrogenation step, caused by a decrease in the Pt-Pt interatomic distance in the Pt shell layer. This indicates that, for a one monolayer coverage of the Pt shell, compression of the Pt lattice is key to the catalysis observed for methanol oxidation.

3.2.3. MOR at $Ru_{core}@Pt_{shell}$ NPs with Pt_{shell} coverages of 1-2 MLs

The electronic properties of the Pt_{shell} are not only affected by the Pt interatomic distance within the shell, but also by the Pt shell thickness. However, the effect of the Ru_{core} on the electronic properties of the Pt_{shell} surface atoms decreases as the Pt_{shell} thickness increases [23]. This is because the outer Pt atoms, at which the MOR occurs, are further away from the Ru_{core} the thicker the Pt_{shell} is. Therefore, if a change in the Pt_{shell} electronic properties is relevant to the MOR kinetics, increasing the Pt_{shell} thickness is expected to result in a noticeable change in the MOR activity of the $Ru_{core}@Pt_{shell}$ NPs. Clearly, the bi-functional mechanism no longer applies, as there are no exposed Ru atoms remaining when the Pt shell coverage is > 1 monolayer, but the Pt-Pt interatomic distance within the shell may change during Pt_{shell} thickening. However, it was shown (Figure 3) that there is an insignificant change in the strain in the Pt_{shell} with increasing thickness of the Pt_{shell} to > 1 ML, and hence the strain effect may be excluded for these thicker Pt shell layers.

The CO intermediate that is produced during methanol oxidation adsorbs strongly to the Pt surface sites, blocking them from further adsorption/oxidation of methanol [66]. Based on the CO stripping results shown in Figure 6 (inset), our previous results[48], and those reported in other studies [23, 28, 67], Ru has a very strong electronic effect on Pt, resulting in a

ca. -200 mV shift in the CO stripping potential when the Ru NPs are covered with a Pt_{shell} monolayer. However, this strong electronic effect of Ru on the Pt_{shell} properties not only weakens the CO-Pt bond, but it also weakens the CH_3OH-Pt bond. Therefore, this is expected to increase the rate of CO oxidation, while decreasing the methanol adsorption/dehydrogenation rate.

The MOR activity of the Ru_{core} and $Ru_{core}@Pt_{shell}$ (EG) catalysts per mass of Pt, with the Pt coverages in the range of 1 to 2 MLs, was therefore examined using cyclic voltammetry (0.05-0.9 V vs. RHE, 20 mV/sec) at both RT (Figure 7a) and 60 °C (Figure 7b) in 1 M CH_3OH + 0.5 M H_2SO_4. In this part of the work, the Ru cores were totally covered with Pt[48], resulting in similar theoretical specific surface areas (based on the TEM determined NP sizes) of 119, 108, and 95 m^2/g for the $Ru_{48}@Pt_{52}$ (1.1, EG), $Ru_{38}@Pt_{62}$ (1.45, EG), and $Ru_{38}@Pt_{62}$ (1.9, EG), respectively. Therefore, if the catalytic activity had been normalized to the total mass of metal in the NPs, it should have shown a similar trend to what was obtained here when the activities were normalized to the Pt area.

Figures 7a and 7b show that the $Ru_{48}@Pt_{52}$ (1.1, EG) NPs have a lower catalytic activity than either the $Ru_{38}@Pt_{62}$ (1.45, EG) or the $Ru_{38}@Pt_{62}$ (1.9, EG) NPs, at both lower and higher potentials. As the electronic effect of the Ru_{core} on the Pt_{shell} surface atoms is lowered by the presence of the underlying Pt monolayer for NPs with Pt shell coverages from 1-2 MLs, the MOR rate is seen to increase significantly at higher potentials, but not to a higher extent than at lower potentials. Since increasing the Pt_{shell} thickness should strengthen the CO-Pt bond and decrease the propensity for CO oxidation [48], the rate of the MOR should also decrease, especially at low potentials, due to CO oxidation inhibition. However, an enhanced MOR activity is seen in Fig. 8a at RT and in Fig. 8b at 60 °C with increasing Pt

shell coverage (1-2 MLs) over the full potential range. This is because increasing the Pt_{shell} thickness not only strengthens CO adsorption at Pt, but also enhances methanol adsorption, which then increases the overall MOR rate.

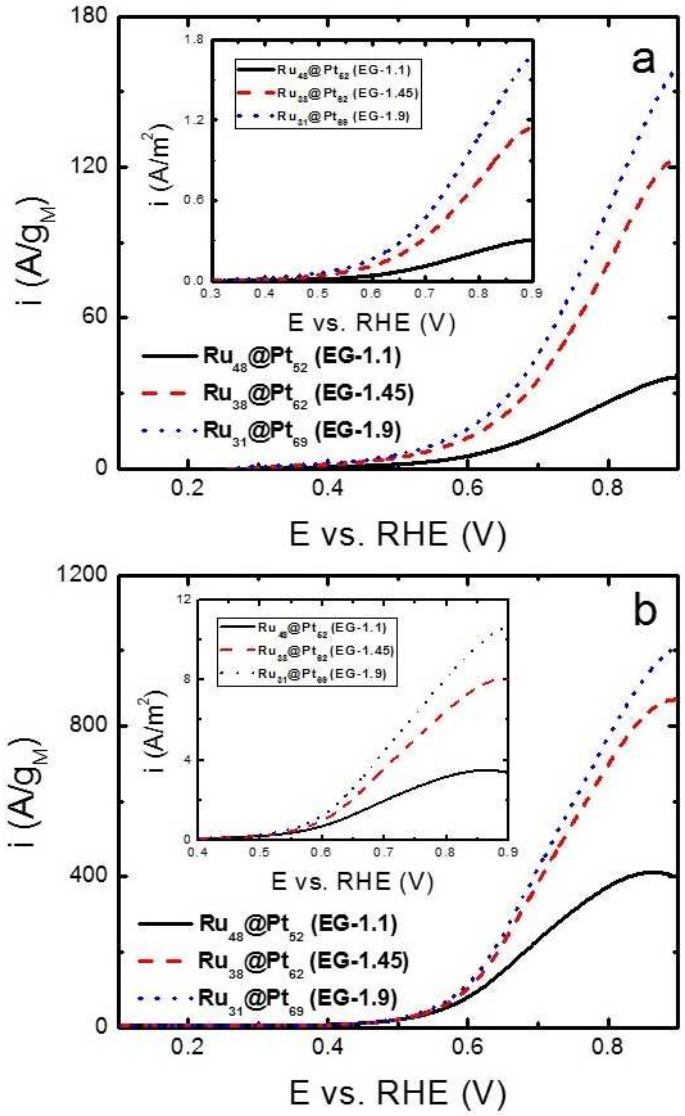

Figure 7: MOR activity at Ru@Pt NP/VC (EG, 2 nm Ru_{core}) catalysts (for Pt_{shell} coverages in the range of 1 to 2 MLs) in the second CV (20 mV/sec) between 0.3 and 0.9 V vs. RHE in 1 M CH_3OH + 0.5 H_2SO_4 at (a) RT and (b) 60 °C. Insets show the catalytic activity divided by the theoretical Pt area (based on TEM-determined particle size).

If the MOR activity of the $Ru_{core}@Pt_{shell}$ NPs, coated with one monolayer of Pt (Figure 5), is high (as in the case of the $Ru_{core}@Pt_{shell}$ (PMG) NPs), the extent of CO build-up should also be high. In this case, the buffering of the Ru electronic effect on the Pt_{shell} by increasing the Pt_{shell} thickness is expected to increase the MOR activity of the $Ru_{core}@Pt_{shell}$ NPs even more at high potentials because of an increase in the rate of methanol adsorption/dehydrogenation. However, the thicker Pt shell should lower the MOR rate at lower potentials through the inhibition of the CO oxidation step.

Figure 8 shows the cyclic voltammograms (0.05-0.9 V vs. RHE, 20 mV/sec) of the $Ru_{core}@Pt_{shell}$ (PMG) NPs with a Pt_{shell} coverage of 1 and 1.5 MLs in RT 1 M CH_3OH + 0.5 M H_2SO_4, with the results at high temperature (60 °C) shown in the inset. At low temperatures, when the Pt coverage increases from 1 to 1.5 ML (Figure 8), the electronic effect of the Ru_{core} on the Pt_{shell} surface atoms has been lowered, which results in a significant increase in the rate of the MOR at high potentials, as expected. However, at lower potentials, an insignificant difference is observed between the MOR activity of the $Ru_{64}@Pt_{36}$ (1.0, PMG) and $Ru_{49}@Pt_{51}$ (1.5, PMG) NPs. At higher temperatures (60 °C), the $Ru_{49}@Pt_{51}$ (1.5, PMG) NPs show a lower activity at low potentials and higher activity at higher potentials, as expected (Fig. 9, inset).

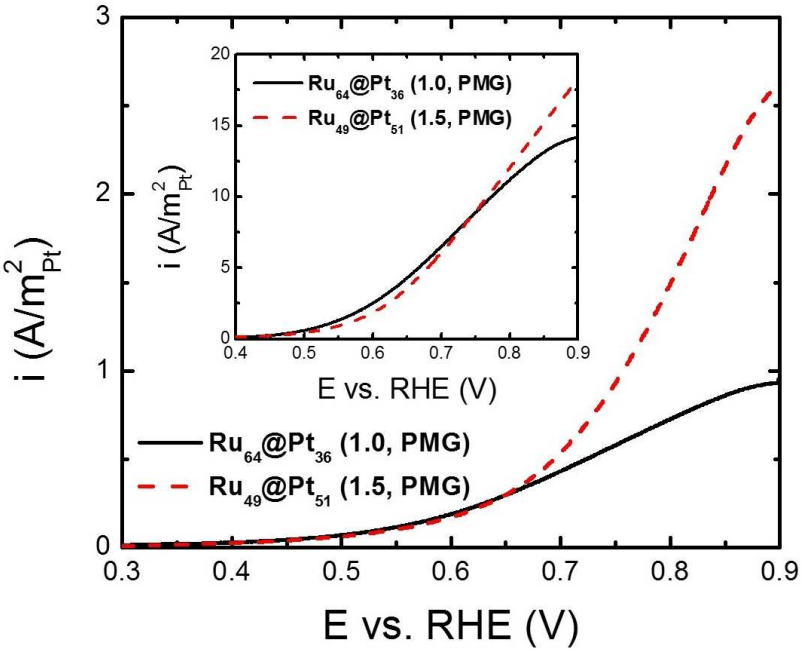

Figure 8: MOR activity of Ru@Pt NP/VC (PMG, 3 nm Ru_{core}) catalysts (for Pt shell coverages of 1 and 1.5 MLs) in the second CV (20 mV/sec) between 0.3 and 0.9 V vs. RHE in 1 M CH_3OH + 0.5 H_2SO_4 at RT and 60 °C (inset).

At low temperatures, the methanol turnover rate and accordingly the rate of CO production is relatively small. Therefore, an inhibition of the CO oxidation reaction by increasing the Pt_{shell} thickness was not observed. At 60 °C, the rate of CO formation is higher than at RT, due to the higher rate of methanol turnover. Thus, it was easier to detect the effect of CO accumulation on the inhibition of the MOR activity in the case of the $Ru_{49}@Pt_{51}$ (1.5, PMG) NPs, as these are less capable of oxidizing CO as compared to the $Ru_{64}@Pt_{36}$ (1.0, PMG) NPs[48].

Overall, it can be concluded that, even when both the Pt and Ru atoms are exposed to the methanolic solution (Pt shell coverage < 1 ML), the bi-functional effect does not significantly affect the MOR rate at $Ru_{core}@Pt_{shell}$ NPs. Instead, it appears that the strain

(compression) that increasingly develops in the Pt_{shell} when the Ru core size is increased can significantly accelerate the rate of the methanol dehydrogenation step, resulting in a large increase in the MOR rate. Also, the electronic effect of the Ru_{core} on the Pt_{shell} properties has been shown here to inhibit the methanol adsorption/dehydrogenation step, but enhance the rate of CO oxidation. Thus, a much improved understanding of the mechanism of the methanol oxidation reaction has been achieved, largely as a result of the careful and reliable design and characterization of the $Ru_{core}@Pt_{shell}$ NPs carried out in the present work.

4. Summary

Pt-Ru alloys are known to be the most promising catalysts for the methanol oxidation reaction (MOR), of relevance to direct methanol fuel cells (DMFCs). However, the role of Ru in enhancing the MOR activity on Pt-Ru catalysts is not fully understood as yet. Thus, in this work, a set of nano-engineered $Ru_{core}@Pt_{shell}$ NPs were synthesized, with the Ru_{core} potentially affecting the Pt_{shell} MOR activity (in 1 M methanol + 0.5 M H_2SO_4 solutions at room temperature to 60 ^oC) through the strain effect, the electronic effect, or the bi-functional effect when the Ru_{core} surface is still exposed (< one monolayer coverage of the Pt shell). To the best of our knowledge, no prior studies have systematically determined which of these effects is dominant during the MOR using well controlled Pt-Ru nanostructures.

In this work, $Ru_{core}@Pt_{shell}$ NPs, having a controlled Pt_{shell} coverage within each monolayer (ML) and a thickness of up to two MLs, as well as two different Ru_{core} sizes (2 and 3 nm), were synthesized using the simple polyol method. When the Pt shell coverage was < 1 monolayer (ML) in thickness, the exposed Ru surface atoms were expected to play a critical role (through the formation of RuOH) in removing CO from Pt (the 'bifunctional'

effect). However, due to the slow rate of regeneration of adsorbed OH, only an improvement in the MOR activity was seen at high temperatures when low Pt coverages were investigated. In general, decreasing the Pt_{shell} coverage and exposing more of the Ru_{core} surface atoms to the methanolic solution was found to result in a decrease in the $Ru_{core}@Pt_{shell}$ NP MOR activity.

When the Ru_{core} NPs were covered with a full ML of the Pt_{shell}, the rate of the MOR showed a significant dependence on the Pt-Pt interatomic strain. The $Ru_{core}@Pt_{shell}$ NPs having a larger (3 nm) Ru_{core} size (highly compressed Pt_{shell}) showed a higher (2-4 times) MOR activity than the $Ru_{core}@Pt_{shell}$ NPs with a smaller (2 nm) Ru_{core} size (less compressed Pt shell), due to the enhancement of the methanol adsorption/dehydrogenation step.

The change in the interatomic distances within the Pt_{shell} results in the presence of both strain and electronic effects. In order to determine which of these is dominant in enhancing the rate of the MOR, the catalytic activity of $Ru_{core}@Pt_{shell}$ NPs coated with a single ML Pt_{shell} was investigated. When the electronic effect of the Ru_{core} on the Pt_{shell} was decreased by increasing the Pt_{shell} thickness, an enhancement in the methanol adsorption step and an inhibition in the CO oxidation step were observed. Finally, it was also shown that the bi-functional mechanism plays only a minor role during the MOR at the $Ru_{core}@Pt_{shell}$ NPs under investigation here.

Acknowledgements

We are very grateful to the Natural Sciences and Engineering Research Council of Canada (NSERC), through its Discovery Grant and CRD granting programs, for the overall support

of this work. We also thank Dr. Tobias Fürstenhaupt (Microscopy and Imaging Facility (MIF), University of Calgary, Alberta, Canada) for help with the TEM/EDX analyses and Dr. Robert A. Marr (The University of Calgary Laboratory for Electron Microprobe Analysis (UCLEMA), Alberta, Canada) for assistance with the WDS analyses.

References:

1. Ye, S., CO-tolerant catalysts. In *PEM Fuel Cell Electrocatalysts and Catalyst Layers: Fundamentals and Applications*, Zhang, J., Ed. Springer: 2008; pp 759-834.
2. Wang, Z.-C.; Ma, Z.-M.; Li, H.-L., Functional multi-walled carbon nanotube/polysiloxane composite films as supports of PtNi alloy nanoparticles for methanol electro-oxidation. *Applied Surface Science* **2008,** 254, (20), 6521-6526.
3. Antolini, E.; Salgado, J. R. C.; Gonzalez, E. R., The methanol oxidation reaction on platinum alloys with the first row transition metals: The case of Pt-Co and -Ni alloy electrocatalysts for DMFCs: A short review. *Applied Catalysis B: Environmental* **2006,** 63, (1-2), 137-149.
4. Park, K.-W.; Choi, J.-H.; Kwon, B.-K.; Lee, S.-A.; Sung, Y.-E.; Ha, H.-Y.; Hong, S.-A.; Kim, H.; Wieckowski, A., Chemical and Electronic Effects of Ni in Pt/Ni and Pt/Ru/Ni Alloy Nanoparticles in Methanol Electrooxidation. *The Journal of Physical Chemistry B* **2002,** 106, (8), 1869-1877.
5. Chu, D.; Gilman, S., Methanol Electro-oxidation on Unsupported Pt-Ru Alloys at Different Temperatures. *Journal of The Electrochemical Society* **1996,** 143, (5), 1685-1690.
6. Park, K.-W.; Choi, J.-H.; Ahn, K.-S.; Sung, Y.-E., PtRu Alloy and PtRuâˆ'WO3 Nanocomposite Electrodes for Methanol Electrooxidation Fabricated by a Sputtering Deposition Method. *The Journal of Physical Chemistry B* **2004,** 108, (19), 5989-5994.
7. Watanabe, M.; Uchida, M.; Motoo, S., Preparation of highly dispersed Pt + Ru alloy clusters and the activity for the electrooxidation of methanol. *J. Electroanal. Chem.* **1987,** 229, (1-2), 395-406.
8. Gasteiger, H. A.; Markovic, N.; Ross, J. P. N.; Cairns, E. J., Temperature-Dependent Methanol Electro-Oxidation on Well-Characterized Pt-Ru Alloys. *Journal of The Electrochemical Society* **1994,** 141, (7), 1795-1803.
9. Jusys, Z.; Kaiser, J.; Behm, R. J., Composition and activity of high surface area PtRu catalysts towards adsorbed CO and methanol electrooxidation--: A DEMS study. *Electrochimica Acta* **2002,** 47, (22-23), 3693-3706.
10. Tsaprailis, H.; Birss, V. I., Sol-Gel Derived Pt-Ir Mixed Catalysts for DMFC Applications. *Electrochemical and Solid-State Letters* **2004,** 7, (10), A348-A352.
11. Lee, K.-S.; Yoo, S. J.; Ahn, D.; Jeon, T.-Y.; Choi, K. H.; Park, I.-S.; Sung, Y.-E., Surface Structures and Electrochemical Activities of Pt Overlayers on Ir Nanoparticles. *Langmuir* **2011,** 27, (6), 3128-3137.
12. Holt-Hindle, P.; Yi, Q.; Wu, G.; Koczkur, K.; Chen, A., Electrocatalytic Activity of Nanoporous Pt-Ir Materials toward Methanol Oxidation and Oxygen Reduction. *Journal of The Electrochemical Society* **2008,** 155, (1), K5-K9.
13. Aramata, A.; Kodera, T.; Masuda, M., Electrooxidation of methanol on platinum bonded to the solid polymer electrolyte, Nafion. *Journal of Applied Electrochemistry* **1988,** 18, (4), 577-582.

14. El Sawy, E. N.; Molero, H. M.; Birss, V. I., Methanol Oxidation at Porous Co-Electrodeposited Pt-Ir Thin Films. *Electrochimica Acta* **2014,** 117, (0), 202-210.
15. El Sawy, E. N.; Birss, V. I., Understanding the Role of Ir on the Methanol Oxidation Catalytic Activity of PtxIry Alloy Nanoparticles. *(under preparation)* **2015**.
16. Petrii, O. A., Pt-Ru electrocatalysts for fuel cells: a representative review. *Journal of Solid State Electrochemistry* **2008,** 12, (5), 609-642.
17. Iwasita, T.; Nart, F. C.; Vielstich, W., An FTIR study of the catalytic activity of a 85:15 platinum-ruthenium alloy for methanol oxidation. *Ber. Bunsen-Ges. Phys. Chem.* **1990,** 94, (9), 1030-4.
18. McBreen, J.; Mukerjee, S., In Situ X-Ray Absorption Studies of a Pt-Ru Electrocatalyst. *Journal of The Electrochemical Society* **1995,** 142, (10), 3399-3404.
19. Mukerjee, S.; McBreen, J., Electrocatalysis of methanol and CO oxidation: an in situ XAS study. *Proc. - Electrochem. Soc.* **1997,** 97-13, (Electrode Materials and Processes for Energy Conversion and Storage IV), 36-51.
20. Mukerjee, S.; McBreen, J., Effect of Ru and Sn additions to Pt on the electrocatalysis of methanol oxidation: an in-situ XAS investigation. *New Mater. Fuel Cell Mod. Battery Syst. II, Proc. Int. Symp.,* **1997**, 548-559.
21. Zhang, X. T.; Wang, H.; Key, J. L.; Linkov, V.; Ji, S.; Wang, X. L.; Lei, Z. Q.; Wang, R. F., Strain Effect of Core-Shell Co@Pt/C Nanoparticle Catalyst with Enhanced Electrocatalytic Activity for Methanol Oxidation. *Journal of The Electrochemical Society* **2012,** 159, (3), B270-B276.
22. Strasser, P.; Koh, S.; Anniyev, T.; Greeley, J.; More, K.; Yu, C.; Liu, Z.; Kaya, S.; Nordlund, D.; Ogasawara, H.; Toney, M. F.; Nilsson, A., Lattice-strain control of the activity in dealloyed coreâ€“shell fuel cell catalysts. *Nat Chem* **2010,** 2, (6), 454-460.
23. Schlapka, A.; Lischka, M.; Gross, A.; Kasberger, U.; Jakob, P., Surface strain versus substrate interaction in heteroepitaxial metal layers: Pt on Ru(0001). *Phys. Rev. Lett.* **2003,** 91, (1), 016101.
24. Gyenge, E., Electrocatalytic Oxidation of Methanol, Ethanol and Formic Acid. In *PEM Fuel Cell Electrocatalysts and Catalyst Layers: Fundamentals and Applications*, Zhang, J., Ed. Springer: 2008; pp 165-288.
25. Liu, H.; Zhang, J., *Electrocatalysis of Direct Methanol Fuel Cells: From Fundamentals to Application*. WILEY-VCH Verlag GmbH & Co. KGaA: Weinheim, 2009; p 582.
26. Lu, C.; Rice, C.; Masel, R. I.; Babu, P. K.; Waszczuk, P.; Kim, H. S.; Oldfield, E.; Wieckowski, A., UHV, Electrochemical NMR, and Electrochemical Studies of Platinum/Ruthenium Fuel Cell Catalysts. *The Journal of Physical Chemistry B* **2002,** 106, (37), 9581-9589.
27. Yang, H.; Yang, Y.; Zou, S., In Situ Surface-Enhanced Raman Spectroscopic Studies of CO Adsorption and Methanol Oxidation on Ru-Modified Pt Surfaces. *The Journal of Physical Chemistry C* **2007,** 111, (51), 19058-19065.
28. Alayoglu, S.; Nilekar, A. U.; Mavrikakis, M.; Eichhorn, B., Ru-Pt core-shell nanoparticles for preferential oxidation of carbon monoxide in hydrogen. *Nat Mater* **2008,** 7, (4), 333-338.
29. Muthuswamy, N.; de la Fuente, J. L. G.; Tran, D. T.; Walmsley, J.; Tsypkin, M.; Raaen, S.; Sunde, S.; Ronning, M.; Chen, D., Ru@Pt core-shell nanoparticles for methanol fuel cell catalyst: Control and effects of shell composition. *International Journal of Hydrogen Energy* **2013**, (0), 1-11.
30. Piela, P.; Eickes, C.; Brosha, E.; Garzon, F.; Zelenay, P., Ruthenium Crossover in Direct Methanol Fuel Cell with Pt-Ru Black Anode. *Journal of The Electrochemical Society* **2004,** 151, (12), A2053-A2059.
31. Zelenay, P., Performance Durability of Direct Methanol Fuel Cells. *ECS Transactions* **2006,** 1, (8), 483-495.

32. Sarma, L. S.; Chen, C.-H.; Wang, G.-R.; Hsueh, K.-L.; Huang, C.-P.; Sheu, H.-S.; Liu, D.-G.; Lee, J.-F.; Hwang, B.-J., Investigations of direct methanol fuel cell (DMFC) fading mechanisms. *Journal of Power Sources* **2007,** 167, (2), 358-365.
33. Chung, Y.; Pak, C.; Park, G.-S.; Jeon, W. S.; Kim, J.-R.; Lee, Y.; Chang, H.; Seung, D., Understanding a Degradation Mechanism of Direct Methanol Fuel Cell Using TOF-SIMS and XPS. *The Journal of Physical Chemistry C* **2008,** 112, (1), 313-318.
34. Gancs, L.; Hakim, N.; Hult, B.; Mukerjee, S., Dissolution of Ru from PtRu Electrocatalysts and its Consequences in DMFCs. *ECS Transactions* **2006,** 3, (1), 607-618.
35. Wang, Y.; Toshima, N., Preparation of Pd-Pt bimetallic colloids with controllable core/shell structures. *Journal of Physical Chemistry B* **1997,** 101, (27), 5301-5306.
36. Alayoglu, S.; Eichhorn, B., Rh-Pt Bimetallic Catalysts: Synthesis, Characterization, and Catalysis of Core-Shell, Alloy, and Monometallic Nanoparticles. *Journal of the American Chemical Society* **2008,** 130, (51), 17479-17486.
37. Alayoglu, S.; Nilekar, A. U.; Mavrikakis, M.; Eichhorn, B., Ru-Pt core-shell nanoparticles for preferential oxidation of carbon monoxide in hydrogen. *Nature Materials* **2008,** 7, (4), 333-338.
38. Goto, S.; Hosoi, S.; Arai, R.; Tanaka, S.; Umeda, M.; Yoshimoto, M.; Kudo, Y., Particle-Size- and Ru-Core-Induced Surface Electronic States of Ru-Core/Pt-Shell Electrocatalyst Nanoparticles. *The Journal of Physical Chemistry C* **2014,** 118, (5), 2634-2640.
39. Chen, Y. M.; Yang, F.; Dai, Y.; Wang, W. Q.; Chen, S. L., Ni@Pt core-shell nanoparticles: Synthesis, structural and electrochemical properties. *Journal of Physical Chemistry C* **2008,** 112, (5), 1645-1649.
40. Luo, J.; Wang, L.; Mott, D.; Njoki, P. N.; Lin, Y.; He, T.; Xu, Z.; Wanjana, B. N.; Lim, I. I. S.; Zhong, C. J., Core/Shell Nanoparticles as Electrocatalysts for Fuel Cell Reactions. *Advanced Materials* **2008,** 20, (22), 4342-4347.
41. Zhou, S. H.; Varughese, B.; Eichhorn, B.; Jackson, G.; McIlwrath, K., Pt-Cu core-shell and alloy nanoparticles for heterogeneous NOx, reduction: Anomalous stability and reactivity of a core-shell nanostructure. *Angewandte Chemie-International Edition* **2005,** 44, (29), 4539-4543.
42. Chen, T.-Y.; Luo, T.-J. M.; Yang, Y.-W.; Wei, Y.-C.; Wang, K.-W.; Lin, T.-L.; Wen, T.-C.; Lee, C. H., Core Dominated Surface Activity of Core-Shell Nanocatalysts on Methanol Electrooxidation. *The Journal of Physical Chemistry C* **2012,** 116, (32), 16969-16978.
43. Wang, R.; Wang, H.; Wei, B.; Wang, W.; Lei, Z., Carbon supported Pt-shell modified PdCo-core with electrocatalyst for methanol oxidation. *International Journal of Hydrogen Energy* **2010,** 35, (19), 10081-10086.
44. Yang, L.; Chen, J.; Zhong, X.; Cui, K.; Xu, Y.; Kuang, Y., Au@Pt nanoparticles prepared by one-phase protocol and their electrocatalytic properties for methanol oxidation. *Colloids and Surfaces A: Physicochemical and Engineering Aspects* **2007,** 295, (1â€“3), 21-26.
45. Chen, T.-Y.; Lin, T.-L.; Luo, T.-J. M.; Choi, Y.; Lee, J.-F., Effects of Pt Shell Thicknesses on the Atomic Structure of Ru–Pt Core–Shell Nanoparticles for Methanol Electrooxidation Applications. *ChemPhysChem* **2010,** 11, (11), 2383-2392.
46. Bokach, D.; de la Fuente, J. L. G.; Tsypkin, M.; Ochal, P.; Endsjø, I. C.; Tunold, R.; Sunde, S.; Seland, F., High-Temperature Electrochemical Characterization of Ru Core Pt Shell Fuel Cell Catalyst. *Fuel Cells* **2011,** 11, (6), 735-744.
47. Tsypkin, M.; de la Fuente, J. L. G.; Garcia Rodriguez, S.; Yu, Y.; Ochal, P.; Seland, F.; Safonova, O.; Muthuswamy, N.; Ronning, M.; Chen, D.; Sunde, S., Effect of heat treatment on the electrocatalytic properties of nano-structured Ru cores with Pt shells. In 2013; Vol. 704, pp 57-66.

48. El Sawy, E. N.; El-Sayed, H. A.; Birss, V. I., Novel electrochemical fingerprinting methods for the precise determination of Ptshell coverage on Rucore nanoparticles. *Chemical Communications* **2014,** 50, (78), 11558-11561.
49. Hsieh, Y.-C.; Zhang, Y.; Su, D.; Volkov, V.; Si, R.; Wu, L.; Zhu, Y.; An, W.; Liu, P.; He, P.; Ye, S.; Adzic, R. R.; Wang, J. X., Ordered bilayer ruthenium-platinum core-shell nanoparticles as carbon monoxide-tolerant fuel cell catalysts. *Nat Commun* **2013,** 4.
50. Hu, S.; Xiong, L.; Ren, X.; Wang, C.; Luo, Y., Pt-Ir binary hydrophobic catalysts: Effects of Ir content and particle size on catalytic performance for liquid phase catalytic exchange. *International Journal of Hydrogen Energy* **2009,** 34, (20), 8723-8732.
51. Vij, D. R.; Lee, H.-L.; Flynn, N., X-ray Photoelectron Spectroscopy. In *Handbook of Applied Solid State Spectroscopy*, Springer US: 2006; pp 485-507.
52. El Sawy, E. N. Development of Nano-Structured Direct Methanol Fuel Cell Anodes University of Calgary, Canada, 2013.
53. Alayoglu, S.; Zavalij, P.; Eichhorn, B.; Wang, Q.; Frenkel, A. I.; Chupas, P., Structural and Architectural Evaluation of Bimetallic Nanoparticles: A Case Study of Pt-Ru Core-Shell and Alloy Nanoparticles. *ACS Nano* **2009,** 3, (10), 3127-3137.
54. William D. Casllister, J., *Materials Science and Engineering: An Introduction*. 6th ed.; John Wiley & Sons, Inc.: 2004.
55. Ma, C. H.; Huang, J. H.; Chen, H., Residual stress measurement in textured thin film by grazing-incidence X-ray diffraction. *Thin Solid Films* **2002,** 418, (2), 73-78.
56. Maillard, F.; Pronkin, S.; Savinova, E. R., Size Effects in Electrocatalysis of Fuel Cell Reactions on Supported Metal Nanoparticles. In *Fuel cell catalysis : a surface science approach* Koper, M. T. M., Ed. John Wiley & Sons, Inc.
: 2009.
57. Gasteiger, H. A.; Markovic, N.; Ross, P. N.; Cairns, E. J., Methanol electrooxidation on well-characterized platinum-ruthenium bulk alloys. *The Journal of Physical Chemistry* **1993,** 97, (46), 12020-12029.
58. Yuan, D.; Gong, X.; Wu, R., Decomposition pathways of methanol on the PtAu(111) bimetallic surface: A first-principles study. *J. Chem. Phys.* **2008,** 128, (6), 5.
59. Koper, M. T. M.; Lai, S. C. S.; Herrero, E., Mechanisms of the Oxidation of Carbon Monoxide and Small Organic Molecules at Metal Electrodes. In *Fuel Cell Catalysis*, John Wiley & Sons, Inc.: 2008; pp 159-207.
60. Qin, Z. H.; Lewandowski, M.; Sun, Y. N.; Shaikhutdinov, S.; Freund, H. J., Morphology and CO adsorption on platinum supported on thin Fe 3 O 4 (111) films. *Journal of Physics: Condensed Matter* **2009,** 21, (13), 134019.
61. Cao, D.; Lu, G. Q.; Wieckowski, A.; Wasileski, S. A.; Neurock, M., Mechanisms of methanol decomposition on platinum: A combined experimental and ab initio approach. *Journal of Physical Chemistry B* **2005,** 109, (23), 11622-11633.
62. Hadzi-Jordanov, S.; Angerstein-Kozlowska, H.; Vukovic , M.; Conway, B. E., Reversibility and Growth Behavior of Surface Oxide Films at Ruthenium Electrodes. *Journal of The Electrochemical Society* **1978,** 125, (9), 1471-1480.
63. Kardash, D.; Korzeniewski, C., Temperature Effects on Methanol Dissociative Chemisorption and Water Activation at Polycrystalline Platinum Electrodes. *Langmuir* **2000,** 16, (22), 8419-8425.
64. Joo, J.; Uchida, T.; Cuesta, A.; Koper, M. T. M.; Osawa, M., Importance of Acid-Base Equilibrium in Electrocatalytic Oxidation of Formic Acid on Platinum. *Journal of the American Chemical Society* **2013,** 135, (27), 9991-9994.

65. Xu, J.; Yuan, D.; Yang, F.; Mei, D.; Zhang, Z.; Chen, Y.-X., On the mechanism of the direct pathway for formic acid oxidation at a Pt(111) electrode. *Physical Chemistry Chemical Physics* **2013,** 15, (12), 4367-4376.
66. Beden, B.; Lamy, C.; Bewick, A.; Kunimatsu, K., Electrosorption of methanol on a platinum electrode. IR spectroscopic evidence for adsorbed co species. *J. Electroanal. Chem.* **1981,** 121, 343-347.
67. Ochal, P.; Gomez de la Fuente, J. L.; Tsypkin, M.; Seland, F.; Sunde, S.; Muthuswamy, N.; Ronning, M.; Chen, D.; Garcia, S.; Alayoglu, S.; Eichhorn, B., CO stripping as an electrochemical tool for characterization of Ru@Pt core-shell catalysts. *J. Electroanal. Chem.* **2011,** 655, (2), 140-146.

Clarifying the Role of Ru in Methanol Oxidation at $Ru_{core}@Pt_{shell}$ Nanoparticles

Ehab N. El Sawy[a,b], Hany A. El-Sayed[a,b], and Viola I. Birss[a,*]
[a] Department of Chemistry, University of Calgary, 2500 University Drive N.W. Calgary, Alberta, Canada T2N 1N4
[b] Permanent Address: Physical Chemistry and Corrosion Laboratory, National Research Center (NRC), Dokki, Cairo, Egypt
* To whom correspondence should be addressed; E-mail: birss@ucalgary.ca

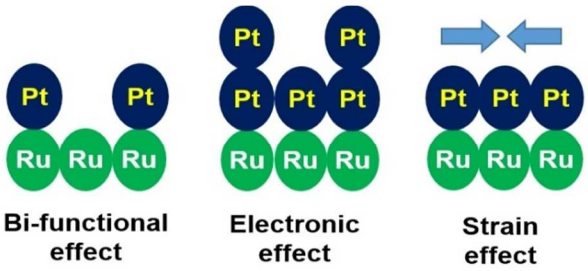

$Ru_{core}@Pt_{shell}$ NPs with a controlled Pt_{shell} coverage and two different Ru_{core} sizes (2 and 3 nm) were synthesized to determine the precise role of Ru on the MOR activity at $Ru_{core}@Pt_{shell}$ NPs.